Coupled Systems Mechanics, *Vol. 7, No. 1 (2018) 95-109*
DOI: https://doi.org/10.12989/csm.2018.7.1.095

The relevance of turbulent mixing in estuarine numerical models for two-layer shallow water flow

Nino Krvavica[**1], Ivica Kožar[*2] and Nevenka Ožanić[1a]

[1]*Department of Hydrology and Hydraulic Engineering, Faculty of Civil Engineering, University of Rijeka, Radmile Matejčić 3, 51000 Rijeka, Croatia*
[2]*Department of Computer Modeling, Faculty of Civil Engineering, University of Rijeka, Radmile Matejčić 3, 51000 Rijeka, Croatia*

(Received May 10, 2017, Revised June 28, 2017, Accepted June 29, 2017)

Abstract. The relevance of turbulent mixing in estuarine numerical models for stratified two-layer shallow water flows is analysed in this paper. A one-dimensional numerical model was developed for this purpose by extending an immiscible two-layer model with an additional source term, which accounts for turbulent mixing effects, namely the entrainment of fluid from the lower to the upper layer. The entrainment rate is quantified by an empirical equation as a function of the bulk Richardson number. A finite volume method based on an approximated Roe solver was used to solve the governing coupled system of partial differential equations. A comparison of numerical results with and without entrainment is presented to illustrate the influence of entrainment on both the salt-water intrusion length and lower layer dynamics. Furthermore, one example is given to demonstrate how entrainment terms may help to stabilize the numerical scheme and prevent a possible loss of hyperbolicity. Finally, the model with entrainment is validated by comparing the numerical results to field measurements.

Keywords: turbulent mixing; entrainment; two-layer flow; finite volume method; shallow water flow; numerical model; estuaries

1. Introduction

Stratified estuaries develop at coastal river mouths where the freshwater flow suppresses the mixing caused by tidal motions (Hansen and Rattray 1966). In these environments, a two-layer flow is usually established, where the freshwater flows downstream towards the river mouth, over a denser saltwater that intrudes upstream. These two layers are separated by a sharp density and salinity gradient, *i.e.*, pycnocline and halocline. A strong vertical stratification occurs in many estuaries worldwide, such as the Mississippi, Merrimack, Fraser, Ebre and Rhone River (Geyer and MacCready 2014, Ibanez *et al.* 1997). Under such conditions, the dynamics of the saltwater propagation may be simulated and predicted by coupled systems of two-layer shallow water

∗Corresponding author, Professor, E-mail: ivica.kozar@uniri.hr
∗∗Corresponding author, Ph.D., E-mail: nino.krvavica@uniri.hr
[a]Professor, E-mail: nozanic@uniri.hr

http://www.techno-press.org/?journal=csm&subpage=8 ISSN: 2234-2184 (Print), 2234-2192 (Online)

equations (Krvavica 2016).

Layered shallow water models are widely used to describe gravity currents (Ungarish 2009), as well as flows in sea straits (Castro *et al.* 2004) and stratified estuaries (Krvavica *et al.* 2017a). These models are usually based on shock-capturing numerical methods and include friction effects. However, turbulent mixing is often neglected from the governing equations. The reason for this may be found in the fact that stratification suppresses the intensity of vertical mixing between the layers. Even for highly dynamics flow conditions, when shear stress is known to locally generate interfacial instabilities and intensify turbulent mixing, the resulting processes occur on a much smaller scale in comparison to the thickness of the upper and lower layer (MacDonald and Geyer 2004). In highly stratified estuaries, however, even a week entrainment may change the dynamics of a nearly-stagnant salt-water layer. Therefore, at least some aspects of the turbulent mixing should be introduced in the governing equations for a two-layer flow.

Krvavica *et al.* (2017) previously presented a one-dimensional numerical model for a two-layer shallow water flow in stratified estuaries. The model accounted for variable channel geometry and shear stress between fluid and channel bed, as well as between two fluids of different density. The proposed model showed satisfactory agreement when compared to field measurements at the Rječina River estuary, especially for near steady-state scenarios. The main drawback of that model was the assumption of immiscible layers, so that no fluid was allowed to cross the interface that separates two layers. The model was later extended by Krvavica *et al.* (2017b), to analyse the response of a stratified estuary to highly dynamics flow conditions, by including the main effects of the turbulent mixing through entrainment, *i.e.*, the vertical transport of salt-water across the interface from a less to a more turbulent layer. The entrainment term resulted in more accurate results, which were confirmed by a comparison to field measurements.

In this paper the relevance of turbulent mixing effects in stratified estuaries, namely entrainment of fluid from the lower to the upper layer, is analysed in more detail. These effects should be noticeable for steady-state solutions, when entrainment may result in lower layer recirculation. Furthermore, entrainment may also help to maintain a locally compromised hyperbolic character of the governing system under highly dynamics flow conditions, when interfacial instabilities are known to appear.

The paper is organized as follows. First, the governing equations for a two-layer shallow water flow with friction and entrainment are derived. Next, a shock-capturing numerical scheme based on the finite volume method is described. And finally, several examples are presented, in which numerical results with and without entrainment are compared to each other and to field measurements at the Rječina River estuary in Croatia.

2. Methodology

2.1 Governing equations

Let us consider two layers of fluid with different densities flowing through a channel defined by arbitrary cross-sections (Fig. 1). In stratified estuaries, the upper layer represents the fresh-water of density ρ_1 and thickness h_1, whereas the lower layer represents the salt-water of density ρ_2 and thickness h_2. An upper layer flows over a denser lower layer towards the river mouth, where internally critical flow is usually established (Krvavica *et al.* 2012, 2017a).

The governing equations for a one-dimensional coupled two-layer shallow water flow in

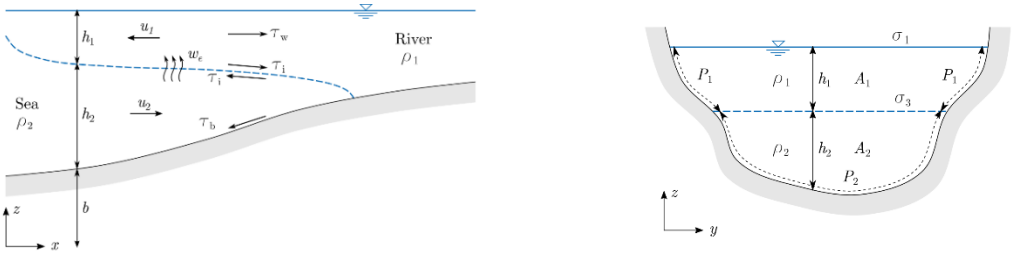

Fig. 1 Longitudinal and cross section of a two-layer flow in a stratified estuary

channels with arbitrary cross-sections, including friction and entrainment, are derived from the conservation laws for the mass and linear momentum.

Under the shallow water hypothesis (White 2003), the following system of hyperbolic partial differential equations (PDE) is obtained (Castro *et al.* 2004, Krvavica 2016)

$$\frac{\partial \mathbf{w}}{\partial t}+\frac{\partial \mathbf{f}(\mathbf{w},\boldsymbol{\sigma})}{\partial x}=\mathbf{B}(\mathbf{w},\boldsymbol{\sigma})\frac{\partial \mathbf{w}}{\partial x}+\mathbf{v}(\mathbf{w},\boldsymbol{\sigma})+\mathbf{g}(\mathbf{w},\boldsymbol{\sigma})+\mathbf{s}(\mathbf{w},\boldsymbol{\sigma}), \tag{1}$$

with the vector of conserved quantities **w** defined as

$$\mathbf{w}=\{A_1 \quad Q_1 \quad A_2 \quad Q_2\}^T, \tag{2}$$

and the flux vector $\mathbf{f}(\mathbf{w},\boldsymbol{\sigma})$ defined as follows

$$\mathbf{f}(\mathbf{w},\boldsymbol{\sigma})=\left\{Q_1 \quad \frac{Q_1^2}{A_1}+\frac{g}{2\sigma_1}A_1^2 \quad Q_2 \quad \frac{Q_2^2}{A_2}+\frac{g}{2\sigma_2}A_2^2\right\}^T, \tag{3}$$

where A_j is the layer wetted cross-section area, $Q_j=A_j u_j$ is the layer flow rate, u_j is the layer horizontal velocity, σ_j is the channel cross section breadth, g is acceleration of gravity, and index $j=1,2$ denotes the respective upper and lower layer. The first source term appears as a result of coupling the two-layer system, in which $\mathbf{B}(\mathbf{w})$ is defined as (Castro *et al.* 2004)

$$\mathbf{B}(\mathbf{w})=\begin{bmatrix}0 & 0 & 0 & 0\\ 0 & 0 & -g\dfrac{A_1}{\sigma_1} & 0\\ 0 & 0 & 0 & 0\\ -g\dfrac{A_2}{\sigma_1} & 0 & 0 & 0\end{bmatrix}, \tag{4}$$

and $r=\rho_1/\rho_2$ is the ratio between the upper and lower layer density. The second source term defines the derivatives of $\boldsymbol{\sigma}$ (Castro *et al.* 2004)

$$\mathbf{v}(\boldsymbol{\sigma},\mathbf{w})=\left\{0 \quad \frac{g}{2}\frac{\partial}{\partial x}\left(\frac{1}{\sigma_1}\right)A_1^2 \quad 0 \quad \frac{g}{2}\frac{\partial}{\partial x}\left(\frac{1}{\sigma_2}\right)A_2^2\right\}^T \tag{5}$$

whereas the third source term defines the irregular channel geometry (Castro *et al.* 2004)

$$\mathbf{g}(\mathbf{w},\boldsymbol{\sigma})=\left\{0 \quad \frac{gA_1}{\sigma_1}\left(I_{3,1}+I_{3,2}\right) \quad 0 \quad \frac{rgA_2}{\sigma_1}I_{3,1}+\frac{gA_2}{\sigma_2}I_{3,2}\right\}^T, \tag{6}$$

where $I_{3,1}$ and $I_{3,2}$ are cross-section geometry integrals (see Castro *et al.* (2004) or Krvavica (2016) for more details). The remaining source term $\mathbf{s} = \mathbf{s}_F + \mathbf{s}_E$ accounts for the respective friction and entrainment, as follows (Krvavica 2016)

$$\begin{aligned} \mathbf{s}_F(\boldsymbol{\sigma}, \mathbf{w}) &= \left\{0 \quad \frac{\tau_w}{\rho_1} P_1 + \frac{\tau_i}{\rho_1}\sigma_3 \quad 0 \quad \frac{\tau_b}{\rho_2} P_2 - \frac{\tau_i}{\rho_2}\sigma_3\right\}^T \text{ and} \\ \mathbf{s}_E(\boldsymbol{\sigma}, \mathbf{w}) &= \left\{\frac{1}{r} E\Delta u \sigma_3 u_1 \quad E\Delta u \sigma_3 \quad -E\Delta u \sigma_3 \quad -u_2 E\Delta u \sigma_3\right\}^T \end{aligned} \tag{7}$$

where P_j is the layer wetted perimeter, τ_w, τ_b and τ_i are the respective wall, bed and interfacial shear stress, $E = w_e/|\Delta u|$ is the entrainment rate, w_e is the entrainment velocity, and $\Delta u = u_1 - u_2$ is the relative velocity difference.

The shear stresses are defined by the quadratic friction law (White 2003)

$$\begin{aligned} \tau_w &= -c_w \rho_1 u_1 |u_1| \\ \tau_b &= -c_b \rho_2 u_2 |u_2| \\ \tau_i &= -c_i \rho_1 (u_1 - u_2)|u_1 - u_2|, \end{aligned} \tag{8}$$

where c_w, c_b and c_i are the respective wall, bed and interfacial friction coefficients, which relate to the Darcy-Weisbach friction factor as $c = \frac{1}{8} f$ (White 2003). The friction factor between fluid and the channel wall/bed is given by the Colebrook and White's equation (White 2003) or Yen's (2002) explicit approximation for wide open channels

$$f = \frac{1}{4}\left[-\log\left(\frac{k_s}{12\mathrm{Re}} + \frac{1.95}{\mathrm{Re}^{0.9}}\right)\right], \tag{9}$$

where k_s is the absolute roughness, $\mathrm{Re} = u_j R_j / \upsilon_j$ is the Reynolds number of the j-th layer, R_j is the layer hydraulic radius, and υ_j is the layer kinematic viscosity. The coefficient between two fluids of different densities is usually given by the Arita and Jirka (1987) equation or by fitting the results to field measurements (Krvavica *et al.* 2016).

The main effects of the turbulent mixing are accounted for by the source term $\mathbf{s}_E(\boldsymbol{\sigma}, \mathbf{w})$ and entrainment rate E which defines the vertical mass and momentum transfer through the interface from a more to a less turbulent layer (Christodoulou 1986). When the upper layer velocity is greater than the lower one $\Delta u > 0$, source term $\mathbf{s}_E$ is positive in the upper layer and negative in the lower layer, and *vice versa*. The entrainment rate may be parametrized by a number of semi-empirical equations, depending on the type and regime of the stratified flow. Most commonly used are the equations by Christodoulou (1986), who found a power-law dependence of E on bulk Richardson number $Ri = g(1-r)h_1/\Delta u^2$, which is defined as follows

$$E = \begin{cases} 0.07 & \text{for } Ri < 10^{-2} \\ 0.007 Ri^{-1/2} & \text{for } 10^{-2} < Ri < 1. \\ 0.007 Ri^{-3/2} & \text{for } Ri > 1 \end{cases} \tag{10}$$

Richardson number represents the ratio of the stratification strength to the velocity shear, i.e., ratio of stabilizing to destabilizing effects. Note that the vertical mixing is included only through the transfer of mass and momentum, whereas the density remains constant in time and space. The assumption of constant density $\rho_i(x,t) = \rho_i$ in each layer is a first step approximation of the turbulent mixing process necessary to derive a governing PDE system in a conservative form. The downside of such an approximation is that densities in both layers are unaffected by the

entrainment of fluid, and in practice only the volume of fluid is conserved inside the domain, instead of the actual mass. However, laboratory and field measurements indicate that in highly stratified environments, the mixing effects are confined to the interfacial layer (MacDonald and Geyer 2004), whose thickness varies according to the intensity of the vertical transport. Therefore, if the thickness of the interfacial layer is much smaller than the thickness of the upper and lower layer, this approximation can be considered as justified.

2.2 Numerical scheme

The governing system (1) is solved by a Finite Volume Method and an approximate Roe solver. Note that the Eq. (1) is not a conservation law, because of source terms on the right-hand size. However, a modified Q-scheme can still be applied to solve this system (Castro *et al.* 2004). The idea of Castro *et al.* (2004) was to treat source terms locally as flux terms. By expanding the following derivative

$$\frac{\partial \mathbf{f}(\boldsymbol{\sigma},\mathbf{w})}{\partial x}=\frac{\partial \mathbf{f}}{\partial \mathbf{w}}\frac{\partial \mathbf{w}}{\partial x}+\frac{\partial \mathbf{f}}{\partial \sigma}\frac{\partial \sigma}{\partial x}=\mathbf{J}(\boldsymbol{\sigma},\mathbf{w})\frac{\partial \mathbf{w}}{\partial x}+\mathbf{v}(\boldsymbol{\sigma},\mathbf{w}), \tag{11}$$

Eq. (1) can be rewritten in the following quasi-linear form (Castro *et al.* 2004)

$$\frac{\partial \mathbf{w}}{\partial t}+\boldsymbol{Q}(\mathbf{w},\boldsymbol{\sigma})\frac{\partial \mathbf{w}}{\partial x}=\mathbf{g}(\mathbf{w},\boldsymbol{\sigma})+\mathbf{s}(\mathbf{w},\boldsymbol{\sigma}), \tag{12}$$

where $\boldsymbol{Q}(\mathbf{w},\boldsymbol{\sigma})=\mathbf{J}(\mathbf{w},\boldsymbol{\sigma})-\mathbf{B}(\mathbf{w},\boldsymbol{\sigma})$ is the global Jacobian matrix. Therefore, a modified Q-scheme can be applied, in which all remaining source terms are upwinded (Krvavica *et al.* 2017b). This method is explicit in time, shock-capturing and second-order accurate for steady solutions (Castro *et al.* 2004).

The following numerical scheme is proposed to solve Eq. (1) (Krvavica 2016)

$$\begin{aligned}\mathbf{w}_i^{n+1}= \quad & \mathbf{w}_i^n+\frac{\Delta t}{\Delta x}\left(\mathbf{f}_{i-1/2}-\mathbf{f}_{i+1/2}\right)+\frac{\Delta t}{2\Delta x}\left[\mathbf{B}_{i-1/2}(\mathbf{w}_i^n-\mathbf{w}_{i-1}^n)+\mathbf{B}_{i+1/2}(\mathbf{w}_{i+1}^n-\mathbf{w}_i^n)\right]\\ & +\frac{\Delta t}{2\Delta x}\left(\mathbf{v}_{i-1/2}+\mathbf{v}_{i+1/2}\right)+\frac{\Delta t}{\Delta x}\left(\mathbf{P}_{i-1/2}^{+}\mathbf{g}_{i-1/2}+\mathbf{P}_{i+1/2}^{-}\mathbf{g}_{i+1/2}\right)\\ & +\Delta t\left(\mathbf{P}_{i-1/2}^{+}\mathbf{s}_{i-1/2}+\mathbf{P}_{i+1/2}^{-}\mathbf{s}_{i+1/2}\right),\end{aligned} \tag{13}$$

where intermediate numerical fluxes are approximated by a Q-scheme (Castro *et al.* 2004)

$$\mathbf{f}_{i+1/2}=\frac{1}{2}[\mathbf{f}(\mathbf{w}_i^n)+\mathbf{f}(\mathbf{w}_{i+1}^n)]-\frac{1}{2}|\boldsymbol{Q}_{i+1/2}|(\mathbf{w}_{i+1}^n-\mathbf{w}_i^n), \tag{14}$$

$$\mathbf{f}_{i-1/2}=\frac{1}{2}[\mathbf{f}(\mathbf{w}_{i-1}^n)+\mathbf{f}(\mathbf{w}_i^n)]-\frac{1}{2}|\boldsymbol{Q}_{i-1/2}|(\mathbf{w}_i^n-\mathbf{w}_{i-1}^n), \tag{15}$$

with $|\boldsymbol{Q}_{i-1/2}|=\boldsymbol{Q}_{i-1/2}^{+}-\boldsymbol{Q}_{i-1/2}^{-}$ and $\boldsymbol{Q}_{i-1/2}^{\pm}=\mathbf{K}_{i+1/2}\boldsymbol{\Lambda}_{i+1/2}^{\pm}\mathbf{K}_{i+1/2}^{-1}$, where $\mathbf{K}_{i-1/2}$ is the matrix whose columns are the eigenvectors of the matrix $\boldsymbol{Q}_{i+1/2}$, and $\boldsymbol{\Lambda}_{i+1/2}$ is a diagonal matrix whose coefficients $\lambda_{i+1/2,l}$ $(1\le l\le 4)$ are the eigenvalues of $\boldsymbol{Q}_{i+1/2}$. The projection matrices for upwinding the source terms are defined as (Castro *et al.* 2004)

$$\mathbf{P}_{i+1/2}^{\pm}=\frac{1}{2}\mathbf{K}_{i+1/2}\left(\mathbf{Id}\pm\operatorname{sgn}(\boldsymbol{\Lambda}_{i+1/2})\right)\mathbf{K}_{i+1/2}^{-1}, \tag{16}$$

$$\mathbf{P}^{\pm}_{i-1/2} = \frac{1}{2}\mathbf{K}_{i-1/2}\left(\mathbf{Id} \pm \mathrm{sgn}(\mathbf{\Lambda}_{i-1/2})\right)\mathbf{K}^{-1}_{i-1/2}, \tag{17}$$

where **Id** is the 4×4 identity matrix. Note that the projection matrices are also derived from the eigenvalues of the matrix $\boldsymbol{Q}_{i+1/2}$. The analytical solutions for the eigenvalues are non-trivial, therefore the QZ algorithm (Moler and Stewart 1973) was used for their computation.

The intermediate values (denoted by index $i + 1/2$) are computed at intercells to linearise the system. The Roe's approximations for intermediate states are defined as follows (Castro *et al.* 2004)

$$\mathbf{w}_{i+1/2} = \left\{A_{i+1/2,1} \quad Q_{i+1/2,1} \quad A_{i+1/2,2} \quad Q_{i+1/2,2}\right\}^T, \tag{18}$$

where

$$u_{i+1/2,j} = \frac{u^n_{i,j}\sqrt{A^n_{i,j}} + u^n_{i+1,j}\sqrt{A^n_{i+1,j}}}{\sqrt{A^n_{i,j}} + \sqrt{A^n_{i+1,j}}}, \tag{19}$$

$$A_{i+1/2,j} = \frac{A^n_{i,j} + A^n_{i+1,j}}{2}, \quad Q_{i+1/2,j} = u_{i+1/2,j}A_{i+1/2,j}, \tag{20}$$

$$\sigma_{i+1/2,1} = \frac{\sigma^n_{i,1} + \sigma^n_{i+1,1}}{2}, \quad \sigma_{i+1/2,3} = \frac{\sigma^n_{i,3} + \sigma^n_{i+1,3}}{2}, \quad \frac{1}{\sigma_{i+1/2,2}} = \frac{1-r}{\sigma_{i+1/2,3}} + \frac{r}{\sigma_{i+1/2,1}}, \tag{21}$$

and also

$$\boldsymbol{Q}_{i+1/2} = \mathbf{J}_{i+1/2} - \mathbf{B}_{i+1/2}, \tag{22}$$

where matrices $\mathbf{J}_{i+1/2}$ and $\mathbf{B}_{i+1/2}$ correspond to $\mathbf{J}(\mathbf{w}_{i+1/2}, \boldsymbol{\sigma}_{i+1/2,j})$ and $\mathbf{B}(\mathbf{w}_{i+1/2}, \boldsymbol{\sigma}_{i+1/2,j})$, respectively.

Note that to exactly preserve the steady-state solution for water at rest (the so-called C-property, defined by Bermudez and Vazquez 1994), the following equality must be true at every time step (Castro *et al.* 2004)

$$\boldsymbol{Q}_{i+1/2}(\mathbf{w}_{i+1} - \mathbf{w}_i) = \mathbf{f}(\mathbf{w}_{i+1}) - \mathbf{f}(\mathbf{w}_i) - \mathbf{v}_{i+1/2} - \mathbf{B}_{i+1}(\mathbf{w}_{i+1} - \mathbf{w}_i). \tag{23}$$

The C-property (23) is satisfied when $\mathbf{v}_{i+1/2} = \{0 \quad v_{i+1/2,1} \quad 0 \quad v_{i+1/2,2}\}^{\mathrm{T}}$, where (Castro *et al.* 2004)

$$v_{i+1/2,j} = \frac{g}{2}\left(\frac{1}{\sigma^n_{i+1,j}} - \frac{1}{\sigma_{i+1/2,j}}\right)\left(A^n_{i+1,j}\right)^2 + \frac{g}{2}\left(\frac{1}{\sigma_{i+1/2,j}} - \frac{1}{\sigma^n_{i,j}}\right)\left(A^n_{i,j}\right)^2, \quad j = 1{,}2. \tag{24}$$

The source term corresponding to irregular geometry is first simplified by replacing the integrals by the corresponding derivatives, which gives the following expression (Castro *et al.* 2004)

$$\mathbf{g}(\boldsymbol{\sigma}, \mathbf{w}) = \begin{Bmatrix} 0 \\ gA_1\left[\frac{1}{\sigma_1}\frac{\partial}{\partial x}(A_1 + A_2) - \frac{\partial}{\partial x}(b + h_2 + h_1)\right] \\ 0 \\ gA_2\left[\frac{1}{\sigma_2}\frac{\partial A_2}{\partial x} + \frac{r}{\sigma_1}\frac{\partial A_1}{\partial x} - \frac{\partial}{\partial x}(b + h_2 + rh_1)\right] \end{Bmatrix}, \tag{25}$$

where b is the bed elevation, and then the intermediate values of Eq. (25) are approximated as (Castro *et al.* 2004)

$$\mathbf{g}_{i+1/2} = \{0 \quad g_{i+1/2,1} \quad 0 \quad g_{i+1/2,2}\}^T, \tag{26}$$

where

$$\begin{aligned} g_{i+1/2,1} = \quad & g\frac{A_{i+1/2,1}}{\sigma_{i+1/2,1}}\left(A^n_{i+1,1} + A^n_{i+1,2} - A^n_{i,1} - A^n_{i,2}\right) \\ & -gA_{i+1/2,1}\left(b_{i+1} + h^n_{i+1,2} + h^n_{i+1,1} - b_i - h^n_{i,2} - h^n_{i,1}\right), \\ g_{i+1/2,2} = \quad & \frac{gA_{i+1/2,2}}{\sigma_{i+1/2,2}}\left(A^n_{i+1,2} - A^n_{i,2}\right) + \frac{rgA_{i+1/2,2}}{\sigma_{i+1/2,1}}\left(A^n_{i+1,1} - A^n_{i,1}\right) \\ & -gA_{i+1/2,2}\left(b_{i+1} + h^n_{i+1,2} + rh^n_{i+1,1} - b_i - h^n_{i,2} - rh^n_{i,1}\right). \end{aligned} \tag{27}$$

The intermediate states for friction and entrainment terms are approximated in an equivalent manner (Krvavica 2016)

$$\mathbf{s}_{i+1/2} = \{s_{i+1/2,1[1]} \quad s_{i+1/2,1[2]} \quad s_{i+1/2,2[1]} \quad s_{i+1/2,2[2]}\}^T, \tag{28}$$

where

$$\begin{aligned} s_{i+1/2,1[1]} = \quad & \frac{1}{r}E_{i+1/2}\left(u_{i+1/2,1} - u_{i+1/2,2}\right)\sigma_{i+1/2,3}, \\ s_{i+1/2,2[1]} = \quad & -E_{i+1/2}\left(u_{i+1/2,1} - u_{i+1/2,2}\right)\sigma_{i+1/2,3}, \\ s_{i+1/2,1[2]} = \quad & -c_w u_{i+1/2,1}|u_{i+1/2,1}|P_{i+1/2,1} \\ & -c_i\left(u_{i+1/2,1} - u_{i+1/2,2}\right)|u_{i+1/2,1} - u_{i+1/2,2}|\sigma_{i+1/2,3} \\ & +u_{i+1/2,1}E_{i+1/2}\left(u_{i+1/2,1} - u_{i+1/2,2}\right)\sigma_{i+1/2,3}, \\ s_{i+1/2,2[2]} = \quad & -c_b u_{i+1/2,2}|u_{i+1/2,2}|P_{i+1/2,2} \\ & +rc_i\left(u_{i+1/2,1} - u_{i+1/2,2}\right)|u_{i+1/2,1} - u_{i+1/2,2}|\sigma_{i+1/2,3} \\ & -u_{i+1/2,2}E_{i+1/2}\left(u_{i+1/2,1} - u_{i+1/2,2}\right)\sigma_{i+1/2,3}. \end{aligned} \tag{29}$$

2.3 The stability and the loss of hyperbolicity

Explicit numerical schemes are stable only if Δx and Δt satisfy the *Courant-Friedrichs-Lewy* (CFL) condition (Toro 2001). In this case the eigenvalues of the matrix $\boldsymbol{Q}$ are included in a CFL-like condition to ensure the scheme's stability (Castro *et al.* 2004)

$$\max\left(|\lambda_{i+1/2,l}|\right)\frac{\Delta t}{\Delta x} \leq CFL \leq 1.0, \tag{30}$$

with $1 \leq l \leq 4$. Additionally, to prevent the appearance of negative depths in the lower layer when entrainment terms are active, we propose the following upper limit for the entrainment rate

$$E_{i+1/2} \leq \frac{1}{\Delta t}\frac{A_{i+1/2,2}}{\Delta u_{i+1/2}\sigma_{i+1/2,3}}. \tag{31}$$

Eigenvalues of matrix $\boldsymbol{Q}_{i+1/2}$ are categorized as external, which correspond to the barotropic flow, and internal, which correspond to the baroclinic flow (Castro *et al.* 2004). If the signs of internal eigenvalues are the same, the flow is internally supercritical, and if the signs differ, the flow is internally subcritical. However, when one of the eigenvalues becomes equal to zero, the flow is either internally or externally critical. To prevent the loss of numerical viscosity when critical flow appears, the Harten (1984) regularization is applied, which modifies the diagonal coefficients of the matrix $\boldsymbol{\Lambda}_{i+1/2}$. From the definition of the characteristic polynomial $p(\lambda) = \det(\boldsymbol{Q} - \lambda\mathbf{Id})$ it follows that one of the eigenvalues is equal to zero when the following condition is satisfied (Castro *et al.* 2004)

$$G^2 = Fd_1^2 + Fd_2^2 - (1-r)\frac{\sigma_2}{\sigma_3}Fd_1^2Fd_2^2 = 1, \tag{32}$$

with

$$Fd_1^2 = \frac{Q_1^2\sigma_1}{g(1-r)A_1^3}\frac{\sigma_3}{\sigma_2} \quad \text{and} \quad Fd_2^2 = \frac{Q_2^2\sigma_3}{g(1-r)A_2^3}, \tag{33}$$

where Fd_1 and Fd_2 are respective upper and lower layer densimetric Froude numbers in channels with arbitrary cross section geometry (Castro *et al.* 2004). Furthermore, it follows that for $G < 1$ the flow is subcritical, and for $G > 1$ the flow is supercritical.

Sometimes internal eigenvalues may become complex and then the system loses its hyperbolic character. This problem is related to the occurrence of shear driven instabilities, such as the Kelvin-Helmholtz or Holmboe waves (Castro *et al.* 2011). In real flows, these instabilities appear under strong shear stress, and they usually initiate interfacial mixing, which then dissipates some of the turbulent energy. Unfortunately, the considered model breaks down if complex eigenvalues appear, and cannot simulate unstable flows. However, the numerical scheme can be modified to compute the solutions even in the presence of complex eigenvalues. Castro *et al.* (2011) proposed to apply a real Jacobian decomposition of the matrix $\boldsymbol{Q} = \mathbf{K}^J\boldsymbol{\Lambda}^J(\mathbf{K}^J)^{-1}$, where $\boldsymbol{\Lambda}^J$ is a block diagonal matrix whose blocks are either real eigenvalues or the following 2×2 block

$$\begin{bmatrix} a & b \\ -b & a \end{bmatrix} \tag{34}$$

if the eigenvalues are the complex conjugate numbers $a \pm bi$, and $\mathbf{K}^J$ is the matrix, whose columns are the corresponding eigenvectors. Under this modification the following definition applies $|\boldsymbol{Q}| = \mathbf{K}^J|\boldsymbol{\Lambda}^J|(\mathbf{K}^J)^{-1}$, where $|\boldsymbol{\Lambda}^J|$ is constructed by replacing the eigenvalues by their absolute values if they are real or by replacing the block (Eq. (34)) by the diagonal values computed as the Euclidean norm of the complex conjugate numbers $\sqrt{a^2+b^2}$. However, even if this modification is applied and the numerical scheme is able to march in time in the presence of complex eigenvalues, it may still produce spurious oscillations and eventually blow up (Castro *et al.* 2011).

Another possible solution for the loss of hyperbolicity is given by additional source terms that account for friction effects, which can reduce some of the locally confined shear instabilities through the reduction of velocities. The practical problem is that too much friction may result in excessively diffused results and even produce unphysical oscillations in the flow. A different strategy (Castro *et al.* 2011) was proposed for maintaining the hyperbolic character of the system, by adding extra friction terms only to those cells where complex eigenvalues appeared at a specific time step. However, this method is justified only if instabilities are confined in both space and time.

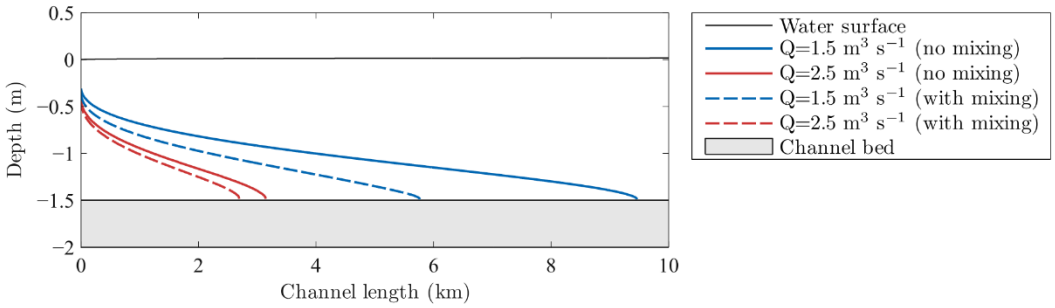

Fig. 2 Computed longitudinal interface profile for Scenario 1 and 2, with and without entrainment

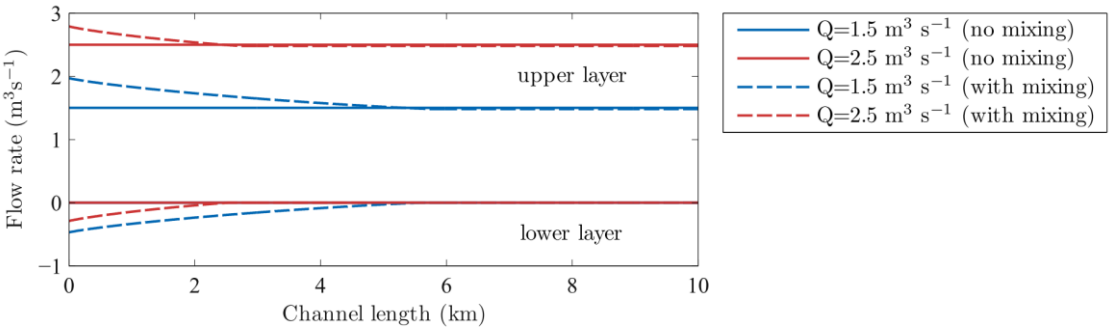

Fig. 3 Computed flow rates in the upper and lower layer for Scenario 1 and 2, with and without entrainment

A general solution to this problem should include a more physically realistic interpretation of interfacial processes. A first step in this direction, is to demonstrate that additional source terms that account for turbulent mixing, *i.e.*, vertical transfer of mass and momentum, can help to maintain the hyperbolic character of the system in cases where strong shear stress usually results in interfacial instabilities and complex eigenvalues in the numerical scheme.

3. Results and discussion

Three numerical tests are presented to illustrate the relevance of the turbulent mixing in a two-layer shallow water flow. First, a steady-state flow with and without entrainment was computed in an ideal channel to show the impact of E on the overall interface profile and lower layer dynamics in a highly stratified estuary. The second example demonstrates the importance of mixing terms when dealing with a possible loss of the hyperbolicity. And finally, the third example is given to validate the proposed model with entrainment by comparing the numerical results with field measurements in the Rječina River estuary.

3.1 Test 1: Steady-state solutions with and without entrainment

A 10 km long horizontal channel was considered, defined by a uniform rectangular cross-section with $\sigma = 20$ m. The spatial step was set to $\Delta x = 10$ m and the time step was chosen to satisfy the stability condition CFL = 0.9, also $g = 9.81\ \mathrm{m\ s^{-2}}$ and $r = 0.975$. The downstream

boundary condition was forced by a constant total depth $H = 1.5$ m, and h_1 was computed from the internally critical flow condition (Eq. (32)). Two scenarios were considered; the upstream boundary condition was forced by a constant flow rate, $Q = 1.5$ m^3 s^{-1} for Scenario 1 and $Q = 2.5$ m^3 s^{-1} for Scenario 2. The bed friction factor was computed from the Yen's Eq. (9), the interfacial friction factor was set to $c_i = 10^{-3}$, and E was computed from the Christodoulou's entrainment Eq. (10). The simulation ran until quasi-steady flow conditions were established.

The numerical solutions - interface profiles and flow rates in both layers - are respectively shown in Figs. 1 and 2. The results suggest that the computed salt-water intrusion length is shorter when entrainment terms are included (Fig. 1). As expected, the influence of entrainment is more pronounced over longer reaches; in Scenario 1 the intrusion length computed by the model with entrainment is L = 5760 m in comparison to L = 9460 m obtained by the model without entrainment, which is almost a 40% decrease; on the other hand, in Scenario 2 the intrusion length difference was 14% (L = 2690 m with entrainment and L = 3140 m without entrainment). These differences are mainly caused by the lower layer dynamics, i.e., the entrainment of fluid from the lower to the upper layer results in a return flow in the lower layer and a gradual increase of the flow in the upper layer. Therefore, steeper interface profiles and shorter intrusion lengths develop as a results of larger velocity differences between the layers. Fig. 2 shows how the flow rates in both layers gradually increase in the downstream direction. For Scenario 1 and the river flow rate $Q = 1.5$ m^3 s^{-1}, the computed flow rates at the mouth were $Q_1 = 1.97$ m^3 s^{-1} in the upper layer and $Q_2 = -0.47$ m^3 s^{-1} in the lower layer. For Scenario 2 and the river flow rate $Q = 2.5$ m^3 s^{-1}, the computed flow rates at the mouth were $Q_1 = 2.79$ m^3 s^{-1} in the upper layer and $Q_2 = -0.29$ m^3 s^{-1} in the lower layer. Note that the local entrainment rate is larger for Scenario 2 in comparison to Scenario 1, due to higher flow rate, velocity and consequently the Richardson number; however, the overall influence is more pronounced in Scenario 2, because of a longer span of the interface on which the entrainment acts.

3.2 Test 2: Loss of hyperbolicity

To demonstrate the behaviour of the model under a possible loss of hyperbolicity, we considered a sudden freshwater flow rate increase in the Rječina River estuary. As the upper layer flow rate increases, the lower salt-water is gradually driven out of the channel. Since the geometry of Rječina River, especially the bed elevation, is irregular, the propagation of the salt-water front may result in strong velocity differences and a loss of hyperbolicity (Krvavica 2016).

A similar model set-up was used as in the previous example, except that a realistic channel geometry was used instead of an ideal one. The spatial step was set to $\Delta x = 10$ m and the time step was chosen to satisfy CFL = 0.9. The relative density was set to $r = 0.975$, and $g = 9.81$ m s^{-2}. The bed friction factor was computed from the Yen's explicit Eq. (9) and the interfacial friction factor was calibrated to fit the field measurements (Krvavica *et al.* 2016). The entrainment rate E was computed from the Christodoulou's entrainment Eq. (10). The downstream boundary condition was forced by a constant total depth defined by the sea level +0.0 m a.s.l., and h_1 was computed from the internally critical flow condition (Eq. (32)). The upstream boundary condition was forced by a variable flow rate, i.e., an increase from $Q = 4.3$ m^3 s^{-1} at $t = 0$ min to $Q = 9.7$ m^3 s^{-1} at $t = 15$ min.

The numerical results with and without entrainment (applying a real Jordan decomposition) at different time steps are shown in Fig. 3. The initial solution of the longitudinal interface profile is shown in Fig. 3(A) for $Q = 4.3$ m^3 s^{-1}. As the flow rate in the upper layer gradually increases, the

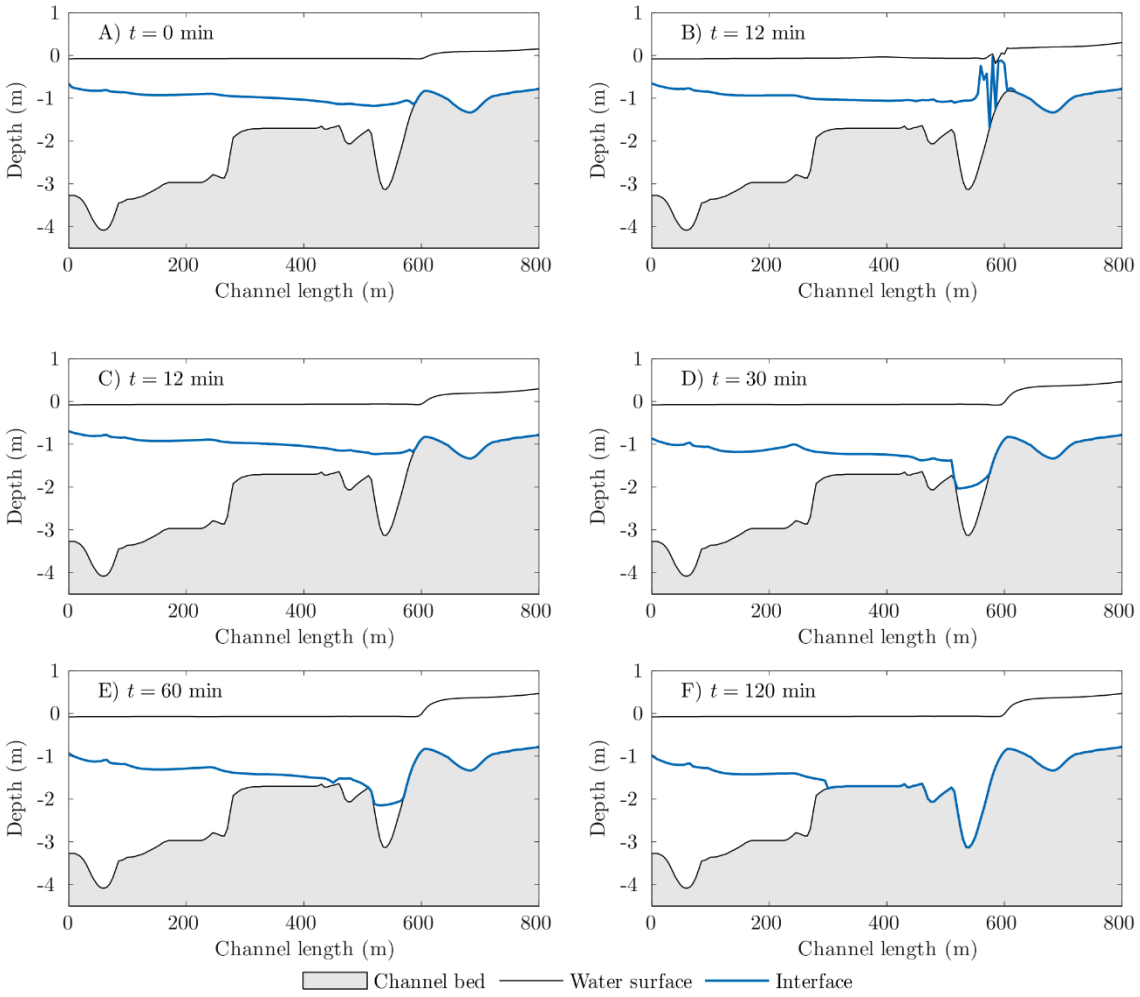

Fig. 4 Test 2: Computed interface profiles in the Rječina River estuary during a freshwater increase from Q = 4.3 m^3 s^{-1} at t = 0 min to Q = 9.7 m^3 s^{-1} at t = 15 min. A) Initial condition, B) result without entrainment, C-F) results with entrainment

lower layer retreats towards the river mouth. At $t = 12$ min the model without entrainment exhibits un-physical oscillations near the front and the solution blows up (Fig. 3(B)). On the other hand, the model with entrainment successfully computed the solution at $t = 12$ min (Fig. 3(C)), and remained stable until $t = 120$ min when steady-state solution was reached (Fig. 3(F)).

3.3 Test 3: Comparison with field measurements

The third test is presented to validate the proposed model with entrainment, by comparing two results to field measurements in the Rječina River Estuary. We considered those scenarios in which near steady-state was reached in the estuary; the flow rate was constant for several hours before the measurements, sea level varied minimally (±2 cm in one hour period), and there was almost no influence of waves and winds. A similar model set-up was used as previously; $\Delta x = 10$ m,

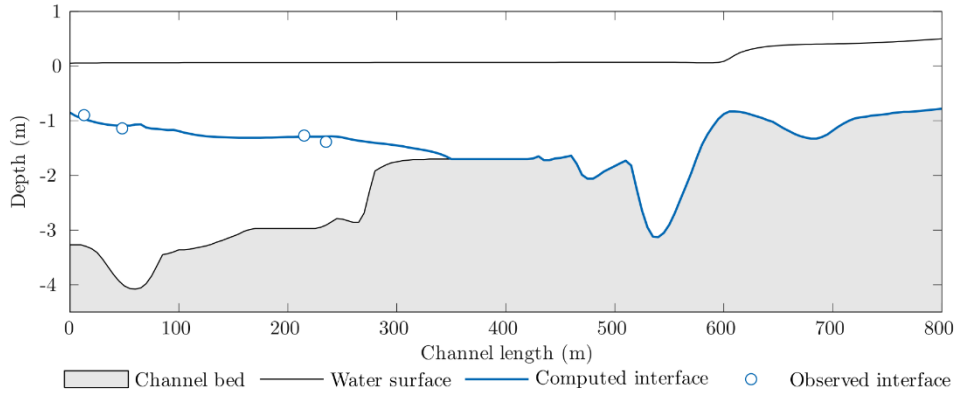

Fig. 5 Test 3, Scenario 1: Computed and observed interface profile in the Rječina River estuary

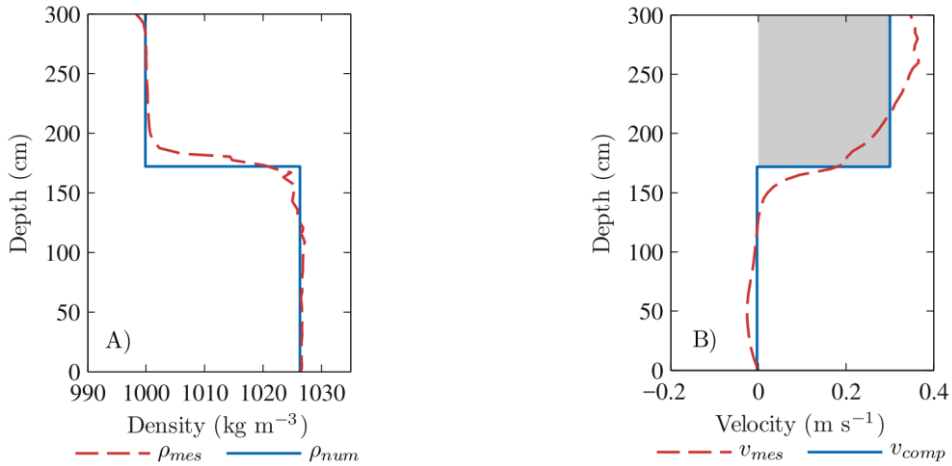

Fig. 6 Test 3, Scenario 1: A) Measured and approximated density profile near the river mouth, B) Measured and computed velocity profile near the river mouth

CFL=0.9, $g = 9.81$ m s^{-2} and $r = 0.974$. The bed friction factor was computed from the Yen's explicit Eq. (9), the interfacial friction factor was calibrated to fit the field measurements (Krvavica *et al.* 2016), and E was computed from the Christodoulou's entrainment Eq. (10). The downstream boundary condition was forced by a constant total depth defined by the sea level +0.05 m a.s.l. for Scenario 1 and -0.04 m a.s.l. for Scenario 2, and h_1 was computed from the internally critical flow condition (Eq. (32)). The upstream boundary condition was forced by constant flow rates, $Q = 9.77$ m^3 s^{-1} for Scenario 1 and 4.36 m^3 s^{-1} for Scenario 2. The simulation ran until quasi-steady flow conditions were established.

The numerical steady-state results are compared to field measurements to validate the proposed model. Fig. 4 shows the computed interface profile in the Rječina River estuary for $Q = 9.77$ m^3 s^{-1} (Scenario 1) and the observed depths of the interface at several points along the estuary. The agreement between the numerical results and field observations is excellent, which should not be surprising since the interfacial friction coefficient was previously calibrated to fit the field measurements (Krvavica *et al.* 2016). Fig. 5(A) shows the measured vertical density profile and

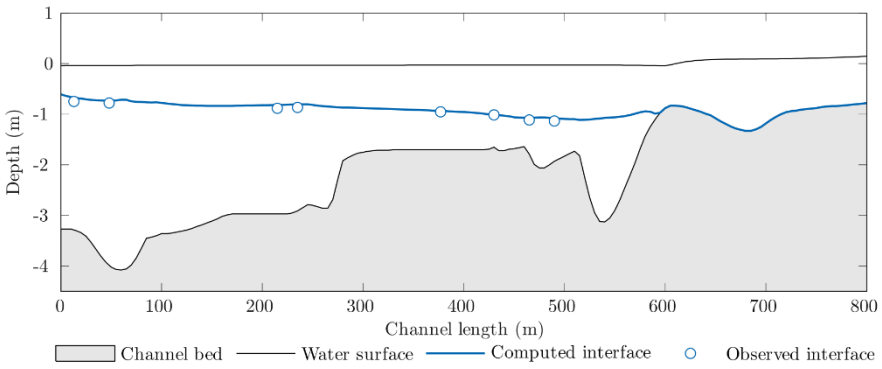

Fig. 7 Test 3, Scenario 2: Computed and observed interface profile in the Rječina River estuary

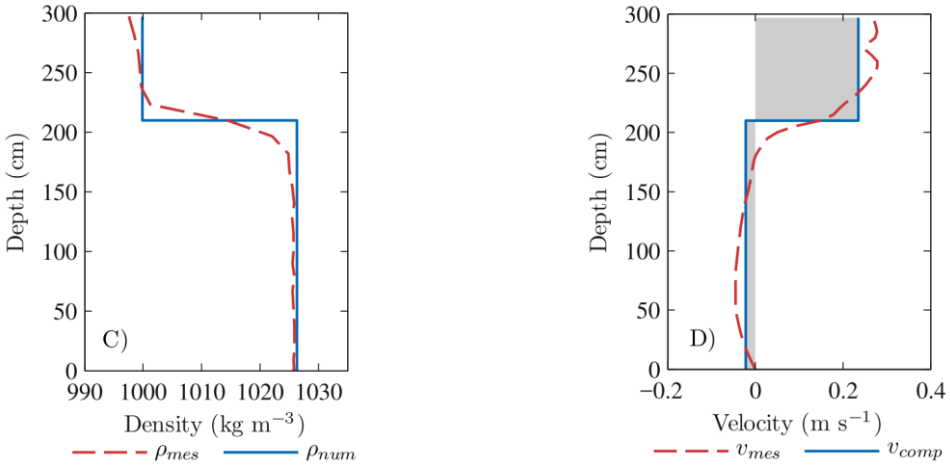

Fig. 8 Test 3, Scenario 2: A) Measured and approximated density profile near the river mouth, B) Measured and computed velocity profile near the river mouth

approximated two-layer profile used as a model input. We can notice a typical two-layer structure with homogeneous upper and lower layer of different densities, and a very thin interface layer (~15 cm) defined by a strong density gradient. This type of profile suggests a stable stratification and week entrainment effects. Fig. 5(B) shows a measured vertical velocity profile near the mouth compared to the computed average velocities in the upper and lower layer. The upper layer shows a typical turbulent profile defined by positive velocities (directed downstream, towards the river mouth), whereas the lower layer is almost stagnant, which additionally confirms week entrainment effects. The agreement between numerical results and measured profiles is satisfactory. Computed flow rates at the mouth were $Q_1 = 9.97$ m^3 s^{-1} in the upper layer and $Q_2 = -0.27$ m^3 s^{-1} in the lower layer.

4. Conclusions

A numerical analysis of turbulent mixing effects in stratified estuaries was presented here. For

this purpose, a one-dimensional numerical model was developed by extending traditional two-layer shallow water models by additional source terms, which accounted for the entrainment of fluid from a less to a more turbulent layer. The entrainment rate can be quantified by several known empirical laws; in this work, the Christodoulou's equations were used, which relate the entrainment rate to the bulk Richardson number. These equations predict that the entrainment rate increases as the Richardson number decreases.

The influence of the turbulent mixing in stratified estuaries was demonstrated by several numerical examples. First numerical test in an ideal prismatic channel showed that even a week entrainment rate may have considerable influence on the computed intrusion length over longer reaches. The entrainment in the model is accounted for by a vertical transport of mass and momentum, which results in a return flow in the lower layer and increased flow in the upper layer. Consequently, the velocity difference between the layer increases and the slope of the interface is steepened. Including entrainment terms may also have beneficiary influence on the stability of the numerical scheme in cases when a loss of hyperbolicity is known to occur. Second example demonstrate one such case, where the model without entrainment displayed unphysical oscillations in the results, whereas the model with entrainment successfully computed the solution at every time step. Finally, the predicted influence of entrainment on initiating the return flow and the lower layer dynamics is confirmed by comparing the numerical results with field measurements in the Rječina River estuary. For short intrusion lengths, entrainment shows almost no effect on the lower layer dynamics. However, over longer reaches, even a week entrainment may result in a return flow in the lower layer. These findings suggest that entrainment, although week in stratified estuaries, is an important aspect of two-layer models, and should be accounted for.

In conclusion, the presented model represents a good compromise between computational speed and accuracy, and as such can be considered a valuable tool in predicting salt-water intrusion in stratified estuaries. The model can be further improved, without significant loss of complexity, by including a third intermediate layer, which should additionally increase its accuracy and physical credibility.

Acknowledgments

This work has been supported in part by Ministry of Science, Education and Sports of the Republic of Croatia under the project Research Infrastructure for Campus-based Laboratories at the University of Rijeka, number RC.2.2.06-0001, which was co-funded from the European Fund for Regional Development (ERDF). The support has also been provided in part by the University of Rijeka under the project Hydrology of Water Resources and Risk Identification from Floods and Mudflows in Karst Areas (13.05.1.1.03).

References

Arita, M. and Jirka, G.H. (1987), "Two-layer model of saline wedge. I: Entrainment and interfacial friction", *J. Hydr. Eng.*, **113**(10), 1229-1246.

Bermudez, A. and Vazquez, M.E. (1994), "Upwind methods for hyperbolic conservation laws with source terms", *Comput. Flu.*, **23**(8), 1049-1071.

Castro, M.J., Fernández-Nieto, E.D., González-Vida, J.M. and Parés-Madronal, C. (2011), "Numerical treatment of the loss of hyperbolicity of the two-layer shallow-water system", *J. Sci. Comput.*, **48**(1-3), 16-

40.
Castro, M.J., García-Rodríguez, J.A., González-Vida, J.M., Macías, J., Parés, C. and Vázquez-Cendón, M.E. (2004), "Numerical simulation of two-layer shallow water flows through channels with irregular geometry", *J. Comput. Phys.*, **195**(1), 202-235.
Christodoulou, G. (1986), "Interfacial mixing in stratified flows", *J. Hydr. Res.*, **24**(2), 77-92.
Geyer, W.R. and MacCready, P. (2014), "The estuarine circulation", *Ann. Rev. Flu. Mech.*, **46**(1), 175-197.
Hansen, D.V. and Rattray, M. (1966), "New dimensions in estuary classification", *Limnol. Oceanogr.*, **11**(3), 319-326.
Harten, A. (1984), "On a class of high resolution total-variation-stable finite-difference schemes", *SIAM J. Numer. Analy.*, **21**(1), 1-23.
Ibàñez, C., Pont, D. and Prat, N. (1997), "Characterization of the ebre and rhone estuaries: A basis for defining and classifying salt-wedge estuaries", *Limnol. Oceanogr.*, **42**(1), 89-101.
Krvavica, N. (2016), "One-dimensional numerical model for layered shallow water flow in highly stratified estuaries", Ph.D. Dissertation, University of Rijeka, Rijeka, Croatia.
Krvavica, N., Kožar, I., Travaš, V. and Ožanić, N. (2017a), "Numerical modelling of two-layer shallow water flow in microtidal salt-wedge estuaries: Finite volume solver and field validation", *J. Hydrol. Hydromech.*, **65**(1), 49-59.
Krvavica, N., Mofardin, B., Ružić, I. and Ožanić, N. (2012), "Measurement and analysis of salinization at the rječina estuary", *Gradevinar*, **64**(11), 923-933.
Krvavica, N., Travaš, V. and Ožanić, N. (2016), "A field study of interfacial friction and entrainment in a microtidal salt-wedge estuary", *Environ. Flu. Mech.*, **16**(6), 1223-1246.
Krvavica, N., Travaš, V. and Ožanić, N. (2017b), "Salt-wedge response to variable river flow and sea-level rise in the microtidal river estuary, Croatia", *J. Coast. Res.*, **33**(4), 802-814.
MacDonald, D.G. and Geyer, W.R. (2004), "Turbulent energy production and entrainment at a highly stratified estuarine front", *J. Geophys. Res.*: *Oceans*, **109**(C5), 1-17.
Moler, C.B. and Stewart, G.W. (1973), "An algorithm for generalized matrix eigenvalue problems", *SIAM J. Numer. Analy.*, **10**(2), 241-256.
Toro, E.F. (2001), *Shock-Capturing Methods for Free-Surface Shallow Flows*, John Wiley, New Jersey, U.S.A.
Ungarish, M. (2009), *An Introduction to Gravity Currents and Intrusions*, CRC Press, Taylor & Francis Group, Florida, U.S.A.
White, F.M. (2003), *Fluid Mechanics*, McGraw-Hill Book Company, New York, U.S.A.
Yen, B.C. (2002), "Open channel flow resistance", *J. Hydraul. Eng.*, **128**(1), 20-39.